Disjoining Pressures and Film Stability of Alkyltrimethylammonium Bromide Foam Films

Vance Bergeron*

Equipe Mixte RP-CEA, Service de Chimie Moléculaire, Centre d'Etudes de Saclay, 91191 Gif sur Yvette, France

Received January 2, 1997. In Final Form: April 10, 1997[⊗]

The alkytrimethylammonium bromide surfactant series, C_nTAB, $n = 10, 12, 14, 16$, is used to perform a systematic study of the forces and stability of foam films produced from soluble cationic surfactants. Both surface tension and disjoining pressure isotherms are measured for each surfactant. This information is then combined with neutron reflectivity and dynamic surface tension results found in the literature to provide an understanding of how the surfactant chain length can effect the forces and stability in thin-liquid films. For stable films, we find good quantitative agreement between the interaction forces measured in foam films and those reported from surface force studies on similar systems. We also find that the surfactant's hydrocarbon chain length and packing can strongly influence film stability. For highly purified surfactants an abrupt increase in film stability is seen when extending the chain length from C_{12}TAB to C_{14}TAB. When an uncharged cosurfactant is present, this stability transition takes place between C_{10}TAB and C_{12}TAB. Both transitions correlate well with changes in the monolayer's cohesive strength, and we outline how monolayer cohesion can play a stabilizing role by dampening both spatial and density fluctuations at the air−water interface.

Introduction

The stability of a foam or an emulsion relies on the stability of the individual films that separate the discontinuous phases. Thus, a great deal of effort has been spent studying the dynamics and stability of individual thin-liquid films.[1,2] Although foams and emulsions are in an absolute sense thermodynamically unstable, it is often found that a particular system can be categorized as a relatively short-lived "dynamically" stabilized system (ca. minutes) or one that can remain stable for very long periods (ca. days to years). Champagne foams are a classic example of the former, while cosmetic creams and food emulsions fall into the later category. This striking difference in a dispersion's lifetime reflects the primary mechanisms that govern the individual film stabilities. In the rapidly coalescing dispersions, the film lifetimes are controlled by the drainage rate of the intervening continuous phase (hydrodynamics), while the long-lived systems require additional time to overcome energy barriers that hold the film in a metastable thermodynamic state. These barriers arise from surface-force interactions created by having two interfaces in close proximity. In fact, for some cases overcoming these energy barriers can take so long that other factors such as Oswald ripening and gas diffusion determine the ultimate lifetime of the dispersion. Clearly, understanding and controlling the energy barriers that inhibit thin-film coalescence has great practical benefits for these dispersed systems.

The first quantitative measurements of the repulsive stabilizing forces (i.e. disjoining pressure isotherms) in individual foam films was performed over 30 years ago by Mysels and Jones.[3] The instrument they used is now referred to as a thin-film balance (TFB) and has evolved from being an exotic experimental technique to a primary research tool for investigating molecular interactions in thin-liquid films.[4,5] Over the years, forces in foam films generated from different anionic and nonionic surfactants have been extensively studied;[6−12] however, work directed toward cationic surfactants and the effect of the surfactant's hydrocarbon chain length is lacking. The present study addresses these two needs. Our aim is to quantify the forces for foam films stabilized by purified cationic surfactants and to investigate the role surfactant chain length plays on these forces and the stability of the films.

Here a homologous series of alkyltrimethylammonium bromide surfactants are studied, $C_nH_{2n+1}N(CH_3)_3Br$, (i.e. C_nTAB), $n = 10, 12, 14, 16$. These surfactants are good candidates for a fundamental study because they can be highly purified, and unlike many classical anionic surfactants (e.g. sodium dodecyl sulfate) they do not risk the severe contamination problems resulting from unwanted side reactions. Furthermore, there exists a vast amount of work on the surface forces between bilayers formed from alkylammonium bromides[13−18] and many of the dynamic[19,20] and equilibrium properties of C_nTAB's at the air−water interface are well documented.[21−28] Therefore, by measuring the surface tension and disjoining pressure

* Current address: Rhône Poulenc Industrialisation, 85, Avenue des Frères Perret, B.P. 62, 69192 Saint Fons Cedex, France.

[⊗] Abstract published in *Advance ACS Abstracts,* June 1, 1997.

(1) Scheludko, A. *Adv. Colloid Interface Sci.* **1967**, *1*, 391.
(2) In *Thin Liquid Films, Fundamentals and Applications*; Ivanov, I. B., Ed.; Marcel Dekker: New York, 1988; Surfactant Science Series Vol. 29.
(3) Mysels, K. J.; Jones, M. N. *Discuss. Faraday Soc.* **1966**, *42*, 42.
(4) Claesson, P. M.; Ederth, T.; Bergeron, V.; Rutland, M. W. *Adv. Colloid Interface Sci.* **1996**, *67*, 119.
(5) Claesson, P. M.; Ederth, T.; Bergeron, V.; Rutland, M. W *Trends Phys. Chem.* **1995**, *5*, 161.
(6) Exerowa, D.; Kolarov, T.; Khristov, Khr. *Colloids Surf.* **1987**, *22*, 171.
(7) Bergeron, V.; Radke, C. J. *Langmuir* **1992**, *8*, 3020.
(8) Bergeron, V.; Fagan, M. E.; Radke, C. J. *Langmuir* **1993**, *9*, 1704.
(9) Bergeron, V.; Radke, C. J. *Colloid Polymer Sci.* **1995**, *273*, 165.
(10) Kolarov, T.; Cohen, R.; Exerowa, D. *Colloids Surf.* **1989**, *42*, 49.
(11) Bergeron, V.; Waltermo, A.; Claesson, P. M. *Langmuir* **1996**, *12*, 1336.
(12) Bergeron, V. *Langmuir* **1996**, *12*, 5751.
(13) Pashley, R. M.; McGuiggan, P. M.; Horn, R. G.; Ninham, B. W. *J. Colloid Interface Sci.* **1988**, *126*, 569.
(14) Pashely, R. M.; Ninham, B. W. *J. Phys. Chem.* **1987**, *91*, 2902.
(15) Parker, J. L.; Yaminsky, V. V.; Claesson, P. M. *J. Phys. Chem.* **1993**, *97*, 7706.
(16) Zorin, Z. M.; Churaev, N. V.; Esipova, N. E.; Sergeeva, I. P.; Sobolev, V. D.; Gasanov, E. K. *J. Colloid Interface Sci.* **1992**, *152*, 170.
(17) Johnson, S. B.; Drummond, C. J.; Scales, P. J.; Nishimura, S. *Langmuir* **1995**, *11*, 2367.
(18) Rutland, M. W.; Parker, J. L. *Langmuir* **1994**, *10*, 1110.
(19) Li, B.; Geeraerts, G.; Joos, P. *Colloids Surf.* **1994**, *88*, 251.
(20) Geeraerts, G.; Joos, P.; Villé, F. *Colloids Surf.* **1995**, *95*, 281.
(21) Lee, E. M.; Thomas, R. K.; Penfold, J.; Ward, R. C. *J. Phys. Chem.* **1989**, *93*, 381.

S0743-7463(97)00004-8 CCC: $14.00

isotherms for this cationic series, we are able to quantitatively compare the repulsive forces between foam films and bilayers while simultaneously investigating the influence of the surfactant's hydrocarbon chain length.

Experimental Section

Materials. The cationic alkyltrimethylammonium bromide surfactants, C_nTAB, n = 10, 12, 14, 16, where purchased from Kodak. These surfactants where recrystallized two or three times with a 50:50 wt % acetone:methanol mixture. Surface tension versus surfactant concentration isotherms for all the surfactants used showed no sign of a minimum after recrystallization, indicating a high level of purity (see Figure 2). Potassium bromide (KBr, Gold Label) was obtained from Aldrich and heated to 500 °C for several hours to drive off surface active impurities. Finally, all solutions where prepared with distilled water that was further passed through a Millipore-MilliQ ultra pure water system.

Surface Tension Measurements. All experiments were carried out at an ambient temperature of 23 ± 1 °C. Surface tension measurements at the air−solution interface were performed via the Wilhelmy method using a rectangular (20 mm × 10 mm) "open-frame" probe made from platinum wire (0.19 mm in diameter) and attached to a sensitive, Hottinger Baldwin Messtechnik (HBM) Type Q11 force transducer. The open-frame probe is needed for these cationic surfactants to eliminate wetting anomalies seen when using plates and other probe geometries. The reproducibility with this system is better than ±0.1 mN/m. Solutions are placed in Teflon troughs, and the measurements are made in an enclosed Plexiglas box to prevent contamination and to maintain a humidified environment. The Teflon trough, platinum probe, and all glassware are cleaned with sulfochromic acid and rinsed with copious amounts of Millipore-MilliQ purified water prior to use.

Disjoining Pressure Measurements. Disjoining pressure isotherms were measured using a modified version of the porous-plate technique, first developed by Mysels and Jones.[3] This device operates by maintaining a balance between capillary and thin-film forces and is thus called a thin-film balance, TFB.[4,5] Single thin-liquid films are formed in a hole drilled through a solution-saturated fritted glass disk which is fused to a 3 mm diameter capillary tube. This film holder is enclosed in a 200 cm^3 hermetically sealed Plexiglas cell with the capillary tube exposed to a constant reference pressure. The solution under investigation is placed in a glass container within the cell to prevent contact and possible contamination with the Plexiglas chamber. Manipulation of the cell pressure with a precise screw-driven syringe pump alters the imposed capillary pressure, P_c, on the film and sets the disjoining pressure, Π. Once equilibrium is established, the aqueous core film thickness, h_{core}, is measured using Scheludko's microinterferometric technique[4,5] in conjunction with the multilayer correction method developed by Duyvis to account for the adsorbed surfactant layers.[29] The thickness of the surfactant layers at the air−water interface was taken from the direct neutron reflectivity measurements of Thomas et al.[21−28] for each surfactant used. Figure 1 displays a schematic of the interfacial structure derived from these neutron reflectivity measurements and the measured width of the Gaussian surfactant-tail density distribution at 1/e of its height, σ_c, is used for the hydrocarbon layer thickness in our optical model. The refractive index of the hydrocarbon layer is taken to be that of the alkane corresponding to the surfactant's hydrocarbon chain length (i.e. n_{C12} = 1.422, n_{C14} = 1.429, n_{C16} = 1.434). Further experimental details can be found elsewhere.[4,5,30]

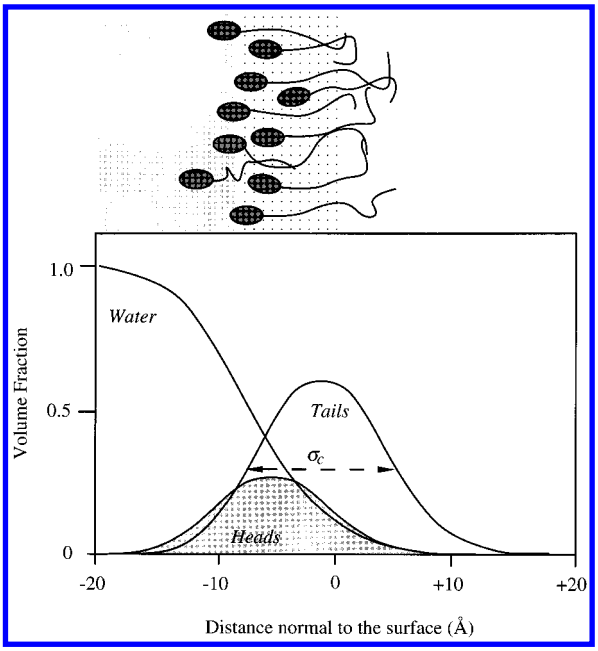

Figure 1. Schematic of the interfacial volume fraction profiles deduced by Thomas et al.[21−28] for C_nTAB surfactant monolayers at the air−water interface.

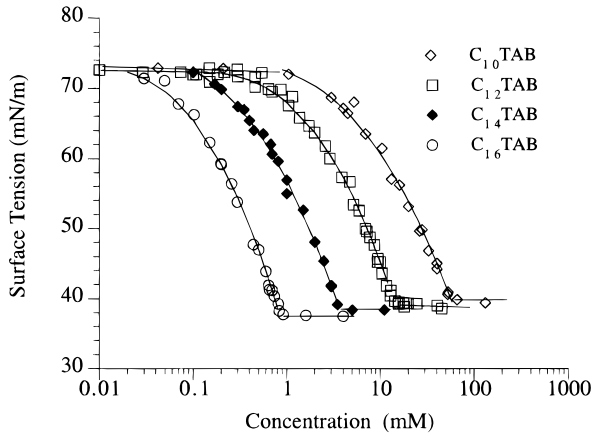

Figure 2. Surface tension versus surfactant concentration isotherms for the C_nTAB surfactants studied. The curved lines represent polynomial fits while the flat lines are sketched in to mark the plateau regions and provide visual continuity of the data.

Results

Surface Tension Isotherms. The surface tension isotherms for all of the surfactants used are displayed in Figure 2. The legend in the figure discriminates the data points, and the curves drawn through these points represent second-order polynomial fits to the data. The straight lines sketched in after the critical micelle concentration, cmc, are provided for visual continuity of the data. As can be seen in Figure 3, the cmc values determined from these isotherms obey the expected logarithmic relationship with increasing chain length and show excellent agreement with literature values.[31,32] Using the polynomial fits to our surface tension isotherms and

(22) Lee, E. M.; Thomas, R. K.; Rennie, A. R. *Prog. Colloid Polym. Sci.* **1990**, *81*, 203.
(23) Simister, E. A.; Thomas, R. K.; Penfold, J.; Aveyard, R.; Binks, B. P.; Cooper, P.; Fletcher, P. D. I.; Lu, J. R.; Sokolowski, A. *J. Phys. Chem.* **1992**, *96*, 1383.
(24) Simister, E. A.; Lee, E. M.; Thomas, R. K.; Penfold, J. *J. Phys. Chem.* **1992**, *96*, 1373.
(25) Lu, J. R.; Simister, E. A.; Lee, E. M.; Thomas, R. K.; Rennie, A. R.; Penfold, J. *Langmuir* **1992**, *8*, 1837.
(26) Lu, J. R.; Simister, E. A.; Thomas, R. K.; Penfold, J. *Prog. Colloid Polym. Sci.* **1993**, *93*, 92.
(27) Lu, J. R.; Hromadova, M.; Simister, E. A.; Thomas, R. K.; Penfold, J. *J. Phys. Chem.* **1994**, *98*, 11519.
(28) Lyttle, D. J.; Lu, J. R.; Su, T. J.; Thomas, R. K.; Penfold, J. *Langmuir* **1995**, *11*, 1001.
(29) Duyvis, E. M. Thesis, Utrecht, 1962.
(30) Bergeron, V. Thesis, University of California, Berkeley, 1993.
(31) Zana, R. *J. Colloid Interface Sci.* **1980**, *78*, 331.
(32) Mukerjee, P.; Mysels, K. J. *Critical Micelle Concentrations of Aqueous Surfactant Systems*; National Bureau of Standards: Washington, DC, 1971.

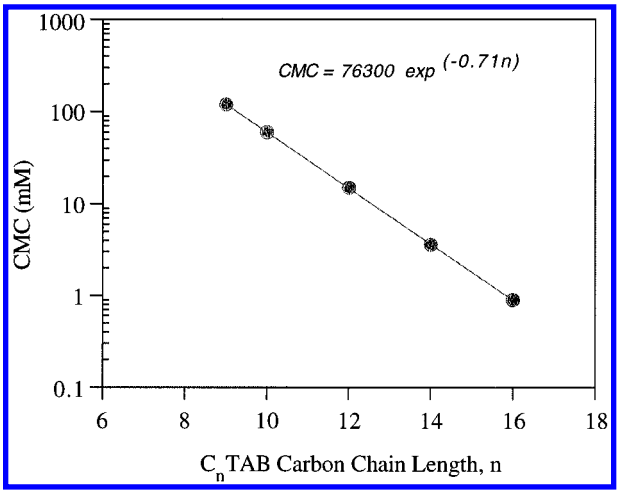

Figure 3. Critical micelle concentration (cmc) versus the C_nTAB carbon chain length, *n*.

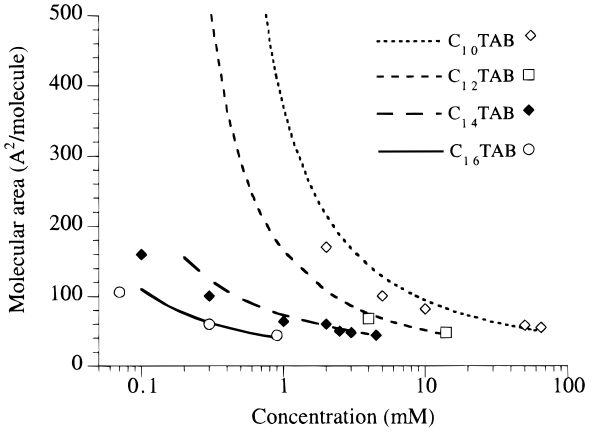

Figure 4. Molecular area at the air−water interface for C_nTAB monolayers. The curves represent data obtained from surface tension isotherms while the discrete points are taken from the neutron reflectivity results of Thomas et al.[21−28]

applying the Gibbs adsorption equation allows it to be used to calculate the molecular area at the air−water interface as a function of the bulk surfactant concentration

$$\Gamma = \frac{1}{\alpha} = -\frac{RT\,d\gamma}{2\,d(\ln c)} \qquad (1)$$

where Γ is the surfactant surface excess, α is the area per molecule, γ is the bulk surface tension, c is the bulk surfactant concentration, R is the gas constant, and T is the temperature. The molecular areas calculated from our data via eq 1 are shown in Figure 4 together with direct measurements of the molecular areas determined by Thomas et al. using neutron reflectivity off the air−water interface.[21−28] Data calculated from the surface tension isotherms are represented in the figure by the continuous lines while the discrete data points correspond to the neutron reflectivity results. The various surfactants are identified in the figure legend. Figure 4 demonstrates excellent agreement between the molecular areas (i.e. adsorptions) determined from our surface tension isotherms and those measured directly by neutron reflectivity. This comparison represents one of the most exhaustive verifications of the Gibbs adsorption equation to date. The slight deviations at the low surfactant concentrations likely arise from the precision of the two measurements in this concentration range. Lastly, we extract the Gibbs or so-called limiting dilatational elasticity, ϵ_0, from our surface tension isotherms by applying, ϵ_0 $= -\Gamma\, d\gamma/d\Gamma$. The calculated elasticities as a function of the bulk surfactant concentration are shown in Figure 5. Again the different surfactants are distinguished in the figure legend and the curves cover the entire concentration range below the cmc.

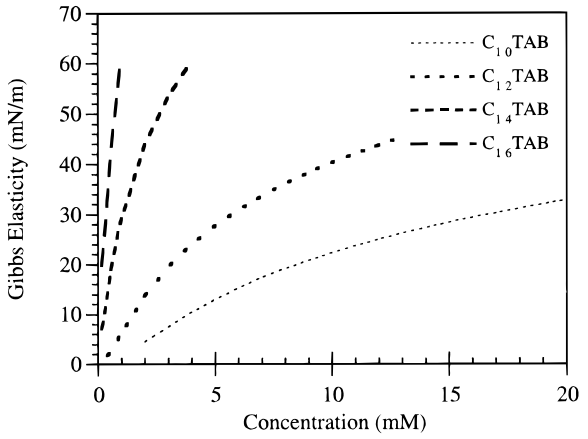

Figure 5. Gibbs elasticity plots for each C_nTAB surfactant tested.

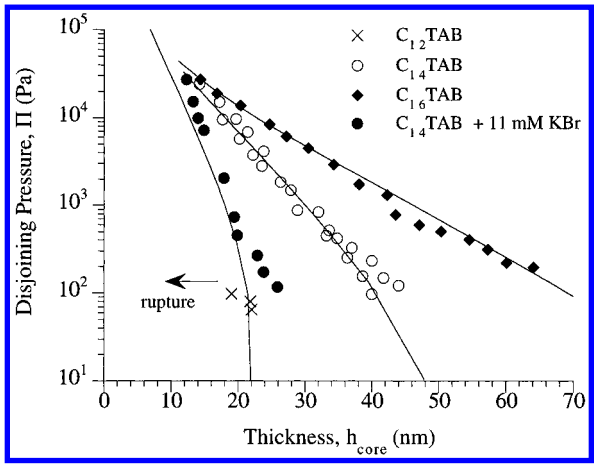

Figure 6. Disjoining pressure versus film thickness for various C_nTAB foam films. In all cases the surfactant concentration is equal to the salt-free cmc and the curves represent constant charge DLVO fits to the data.

Disjoining Pressure Isotherms. Figure 6 displays the disjoining pressure isotherms for foam films obtained from purified solutions of C_{12}TAB (15 mM), C_{14}TAB (3.5 mM), C_{16}TAB (0.9 mM), and C_{14}TAB (3.5 mM) + 11 mM KBr. In each solution the surfactant concentration is equal to the salt-free cmc, and in the last case 11 mM KBr is added to the C_{14}TAB solution so that it has approximately the same ionic strength as the 15 mM C_{12}TAB sample. The data points in the figure represent values from at least two and sometimes three independent measurements, while the solid curves correspond to model fits using DLVO theory imposing constant charge boundary conditions and the theoretical Debye length[33]

$$\kappa^{-1} = \sqrt{\frac{\epsilon^* \epsilon_r kT}{2e^2 z^2 n}}$$

where κ^{-1} is the Debye length, ϵ^* is the permittivity of free space, ϵ_r is the dielectric constant of the film liquid, k is the Boltzmann constant, T is the temperature, e is the electronic charge, z is the ion valency, and n is the ionic

(33) Derjaguin, B. V.; Churaev, N. V.; Muller, V. M. In *Surface Forces*; Kitchener, J. A., Ed.; Consultants Bureau: New York, 1987.

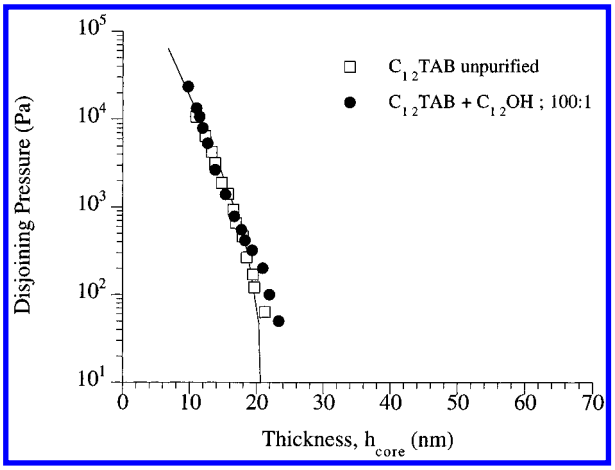

Figure 7. Disjoining pressure versus film thickness for C_{12}TAB foam films at the cmc. The curve corresponds to a constant charge DLVO fit to the data.

concentration. The ionic concentration is set equal to the concentration of surfactant monomer (assuming total dissociation of the monomers in the bulk) plus added salt. Surfactant concentrations are kept low (~cmc) so that corrections to the ionic strength arising from ion binding to micelles are not needed.[14] The parameter extracted from the DLVO fits to our data is the *apparent* surface charge density, σ_0.[34]

Except for C_{12}TAB, all of the disjoining pressure data follow rather classical behavior and film thicknesses decrease with increased imposed pressure in accord with a strong electrical double layer repulsive force. In all cases the films are rather thick, 70−15 nm, and are thus classified as common black films (CBF). Ultrathin Newton Black films (NBF), $h_{core} \approx 0.5$ nm, where never observed even at the maximum imposed pressure of 30 kPa. Likewise the addition of 11 mM KBr to the C_{14}TAB solution only produced CBF films at these pressures. We also note that the C_{14}TAB and C_{16}TAB CBF films are very stable and do not rupture at the highest pressures imposed. To the contrary, data for C_{12}TAB do not continue to higher pressures because these films where unstable and ruptured easily at very low imposed pressures (<1 kPa). Similarly, pure C_{10}TAB solutions produced extremely unstable films, and meaningful pressure−thickness relationships were not even possible. Thus, for pure C_nTAB surfactants at the cmc, we find a significant increase in the film stability between C_{12}TAB and C_{14}TAB.

In contrast to the unstable C_{12}TAB films produced from purified surfactant, unpurified C_{12}TAB (cmc) solutions and purified C_{12}TAB (cmc) solutions with an added long-chain alcohol, C_{12}OH, produced highly stable films. In fact these unpurified films mimic the high stability behavior of the pure C_{14}TAB and C_{16}TAB films. The disjoining pressure isotherms for these two unpure cases are shown in Figure 7. In the alcohol-doped case, C_{12}OH was added to the bulk C_{12}TAB solution at a molecular ratio of 100:1, C_{12}TAB:C_{12}OH. As with the isotherms in Figure 6 the solid curve represents a constant charge DLVO fit to the data and a NBF transition was not observed. The distinguishing features of the isotherms in Figure 7 are the high pressures obtained in contrast to the pure C_{12}TAB surfactant case and the fact that the two data sets produce identical isotherms with the same apparent surface charge density found for pure C_{14}TAB films. An attempt was made to measure isotherms for unpurified C_{10}TAB (cmc) and C_{10}TAB (cmc) solutions doped with long-chain alcohols (C_{10}OH and C_{12}OH); however, films made from these solutions remained too unstable for quantitative measurements. We also note that no difference in the disjoining pressure isotherm was seen between purified and unpurified C_{14}TAB solutions. Therefore a dramatic increase in foam film stability is seen upon increasing the carbon chain from C_{10}TAB to C_{12}TAB in these unpurified samples.

(34) Ennis, J.; Marcelja, S.; Kjellander, R. *Electrochim. Acta* (submitted 1995).

Table 1. DLVO Parameters for C_nTAB Foam Films

	$\psi°$ (mv)	A (Å²/molecule)[a]	σ_0 (C/m²)	β_{film} ($\beta_{micelle}$)[b]
C_{12}TAB	95	46	0.046	0.13 (0.23)
C_{14}TAB	130	46	0.046	0.13 (0.20)
C_{16}TAB	145	43	0.032	0.08 (0.16)

[a] In every case the surfactant concentration is equal to the salt-free cmc. [b] Values taken from ref 31.

Discussion

Disjoining Pressure Isotherms. The interaction curves for the disjoining pressure isotherms shown in Figures 6 and 7 are calculated using DLVO theory. The double-layer repulsion is obtained by solving the nonlinear Poisson−Boltzmann equation, with constant surface charge boundary conditions, using the method of Bell and Petersen.[35] Interfacial charges deduced from these calculations should be regarded as *apparent* values due to the neglect of ion−ion correlation and ion size effects in the Poisson−Boltzmann model. One might expect the real surface charge density to be slightly higher than those obtained from this fitting procedure. Nonetheless, most of the published surface force curves for ammonium bromide bilayers use this same fitting procedure, and thus the apparent values obtained in this study can be readily used for comparison with other similar systems. The van der Waals force for our fits was calculated using the empirical equations of Donners et al.,[36] which represent Lifshitz calculations of a triple-layer foam film (i.e. hydrocarbon−water−hydrocarbon). Consistent with our optical corrections, an alkane with an equivalent chain length and bulk refractive index to the surfactant tails is chosen to model our adsorbed layers. The only films that presented problems with this fitting procedure are those with added electrolyte, C_{14}TAB + 11 mM KBr. The DLVO curve in Figure 6 for this case represents the point at which increasing the surface charge in the model no longer effects the position of the curve (i.e. the charge saturation limit was reached). In this case more sophisticated double-layer models are needed to adequately fit the data.

Table 1 contains the surface charge densities and corresponding potentials extracted from the DLVO fits along with the molecular areas and deduced ionization constants for our foam films. The degree of ionization, β_{film}, is determined directly from our measured surfactant adsorption and surface charge densities. Again we note that the ionization constants are subject to the method used to determine the surface charge and are thus considered *apparent* values. For comparison, ionization constants for the micelles, $\beta_{micelle}$, of these various surfactants are included in parentheses alongside the present values in Table 1. The micellar constants were measured by Zana[31] using a bromide ion specific electrode and/or electrical conductivity. It can be seen that both sets of ionization constants are rather low and that there is a slight decrease with increasing carbon chain length. The small differences between the micelles and the foam films

(35) Bell, G. M.; Petersen, G. J. *J. Colloid Interface Sci.* **1972**, *41*, 542.

(36) Donners, W. A. B.; Rijnbout, J. B.; Vrij, A. *J. Colloid Interface Sci.* **1977**, *60*, 540.

may reflect the spherical geometry of the micelles as opposed to the planar interface of the films, but the precision of the measurements and the approximations involved do not allow us to make definitive conclusions at this level of detail. Interestingly, Johnson et al. have recently found similar trends between micelles and flat bilayers in their study on C_{16}TAB double-layer properties.[17]

A comparison with surface force data from bilayers of C_{16}TAB adsorbed to mica[13] and on glass surfaces[15] support the surface charge and potentials found in the present study. Likewise, excellent agreement is found with the data of Zorin et al. who deduce a 0.035 C/m^2 surface charge for bilayers of C_{16}TAB on quartz.[16] Lastly, Johnson et al. report low ionization constants for C_{16}TAB bilayers ($\beta_{\text{bilayer}} = 0.06$) that are comparable to the values reported here.[17] One advantage in the present work is that no assumptions concerning the molecular area are used to determine β_{film}, instead direct measurements of the molecular adsorption via surface-tension isotherms and independent neutron reflectivity results provide this data.

The low values of the ionization constants may in part result from the simplified double-layer model used; however, neutron reflectivity density profiles of the surfactant at the air−water interface suggest another possible origin. Referring to the interface schematic depicted in Figure 1, which was derived from the neutron reflectivity data of Thomas et al., we see that a significant portion of the surfactant head groups are located in the hydrocarbon rich region of the surfactant tails. Molecular dynamics simulations also confirm this molecular structure of the interface.[37] Since the dielectric constant in this surfactant-tail region is expected to be lower than that of the bulk aqueous solution, the energy for dissociation of the head group ions will be less favorable and hence discourage total dissociation in the interfacial region. To the contrary, total dissociation of the surfactant monomers in the bulk solution is supported by the excellent DLVO fits obtained using a theoretical Debye length based on an ionic strength determined from the bulk surfactant monomer concentration.

Film Stability. Figure 6 dramatically reveals that individual film stability at the cmc is highly dependent on the chain length of the surfactant tail. It was practically impossible to generate films from purified C_{12}TAB solutions at capillary pressures above 1 kPa while solutions of C_{14}TAB and C_{16}TAB resisted rupture at pressures in excess of 30 kPa. Adding 11 mM KBr to the C_{14}TAB solution, thereby matching the ionic strength of the C_{12}TAB solutions, had no destabilizing effect on the C_{14}TAB films. However, unpurified C_{12}TAB films or the addition of small amounts of a long-chain alcohol (C_{12}OH) to the purified C_{12}TAB solutions produced highly stable films that could withstand the maximum imposed pressures (>30 kPa). Although it has long been known that long-chain alcohols can dramatically effect the drainage rate (hydrodynamics) in thin-foam films[38] our observations provide direct evidence that small amounts of alcohol (or surface active contaminates) can have a profound effect on the metastable equilibrium state of the films. This observation is important to our basic understanding of film rupture.

A classical DLVO approach, which simply balances repulsive and attractive interactions across the film, cannot fully explain the film stability behavior witnessed in this study. Focusing on the C_{12}TAB and C_{14}TAB films

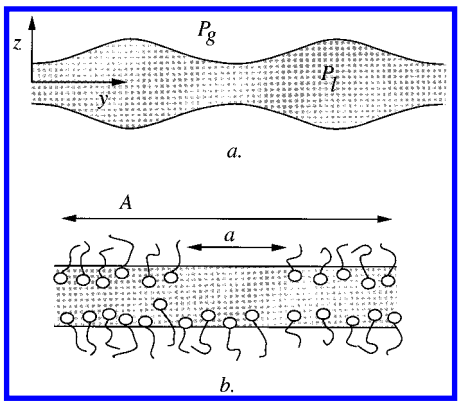

Figure 8. Schematics of the spatial and surfactant density fluctuations in thin-liquid films: (a) a typical spatial fluctuation, (b) a local depletion zone due to monolayer density fluctuations.

we see that the surfactant adsorption in these films is practically identical. Indeed the surfactant adsorption for the entire C_nTAB, $n = 10, 12, 14, 16$, series at the cmc is very similar. Thus, the charge density responsible for the double-layer repulsion should be similar for C_{14}TAB and C_{12}TAB. This is verified in Table 1 for pure C_{14}TAB and unpure C_{12}TAB films. Clearly the ionic strengths (i.e. Debye lengths) are different for each case; therefore, small amounts of salt where added to the C_{14}TAB case to equalize the Debye lengths and bring the stable films into a thickness range where the influence of the attractive van der Waals (destabilizing) forces should also be comparable. This low level of salt has only a small influence on the surfactant adsorption at the cmc; however, even with the added salt the large difference in film stability between the C_{12}TAB and C_{14}TAB films remains. In addition, we point out that the unpurified C_{12}TAB cases should have very similar DLVO force profiles to their pure surfactant counterparts, yet the highly purified case is orders of magnitude less stable. Although repulsive double-layer forces are responsible and necessary for the CBF metastable state of these films, other factors must be considered to completely describe the stability of this state.

When applying DLVO concepts to foam and emulsion films, fluctuations at the interface are often overlooked. Unfortunately a classical DLVO force analysis of film rupture treats the film surfaces as solid uniformly charged non-deforming walls; however, foam and emulsion films have both spatial and surfactant density (i.e. charge) fluctuations occurring at the interface. In reality these fluctuations are superimposed on one another, but for clarity the schematics in Figure 8a,b depict the two cases separately. Since film rupture (and/or a thickness transition) from a metastable state is essentially a nucleated "wetting phase transition", fluctuations can be important near the phase spinodal, as with bulk phase transitions and critical points. Although a complete description of nucleated rupture is beyond the scope of the present work, a simple treatment can provide useful insight into which processes and systems parameters are important. Furthermore, by restricting the complexity we strive to identify "first-order" properties that are readily measurable and thus useful for practical applications.

The original work of Vrij[39,40] has spawned considerable attention concerning the effect spatial fluctuations have on the *spinodal decomposition* of unstable film states; however, the early work of De Vries[41] seems to be one of the few that addresses *nucleated* rupture of rather thick

(37) Böcker, J.; Schlenkrich, M.; Bopp, P.; Brikmann, J. *J. Phys. Chem.* **1992**, *96*, 9915.
(38) Mysels, K. J.; Sinoda, K.; Frankel, S. In *Soap Films-Studies of Their Thinning*; Pergamon Press: New York, 1959.
(39) Vrij, A. *Discuss. Faraday Soc.* **1966**, *42*, 23.
(40) Vrij, A.; Overbeek, J. Th. G. *J. Am. Chem. Soc.* **1968**, *90*, 3074.
(41) De Vries, A. J. *Recl. Trav. Chim. Pays-Bas* **1958**, *77*, 383, 441.

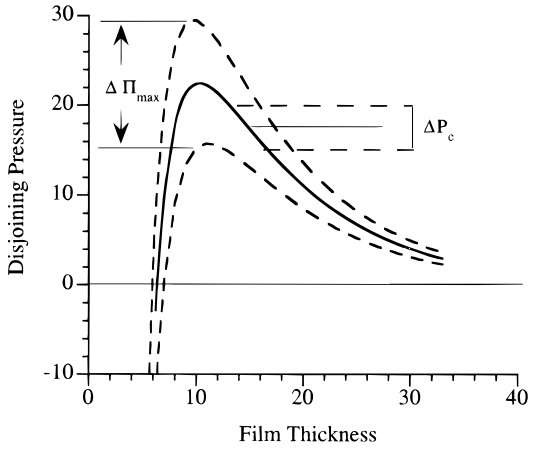

Figure 9. A schematic diagram depicting how capillary pressure, ΔP_c, and disjoining pressure, $\Delta\Pi_{max}$, fluctuations influence the local barrier height relative to the imposed capillary pressure along the film.

foam films (i.e. CBF). Likewise, understanding how surfactant density fluctuations might directly affect the DLVO forces and metastability of foam and emulsion films has received very little attention. We note that nucleated rupture of ultrathin NBF films has been treated, but these films do not undergo thickness variations and are essentially molecular leaflets for which the repulsive disjoining forces are not well understood. Thus, for NBF films it is not clear whether continuum concepts apply (i.e. surface tension, etc.), and the activation energy for film rupture may be governed by different physical parameters.[42−44]

We consider the simple disjoining pressure isotherm in Figure 9 to help understand which film properties control the fluctuations responsible for overcoming the energy barriers that hold our CBF films in a metastable state. This allows use to analyze the process within the framework of familiar DLVO concepts. Clearly other approaches which express the same physical phenomena are possible (e.g. total energy analysis[45]). The solid curve in Figure 9 represents a typical DLVO profile for a system that has one metastable energy minimum (i.e. activation barrier). The dashed lines and curves correspond to how fluctuations influence the disjoining pressure maximum, $\Delta\Pi_{max}$, and variations in the applied capillary pressure, ΔP_c. As with the standard DLVO premise, when the applied pressure exceeds the disjoining pressure, the film has overcome the barrier trapping it in a local thermodynamic minimum. After this point is reached the spinodal decomposition analysis of Vrij[39,40] describing the lifetime of a thermodynamically unstable film is formally applicable. The present objective is to investigate the fluctuations that lead to this unstable stage.

Spatial Fluctuations. The spatial fluctuations shown in Figure 8a manifest themselves as pressure fluctuations along the film, ΔP_c, in Figure 9. The probability of a certain fluctuation depends on the energy expended to create it

$$P_s \approx c_s \exp\left(-\frac{\Delta G_s}{kT}\right) \tag{2}$$

where P_s is the probability of the spatial fluctuation, c_s is a constant, and ΔG_s is the energy expended. For a pure fluid, a simple one-dimensional energy analysis for a sinusoidal fluctuation of the type pictured in Figure 8a was worked out by Vrij and Overbeek.[39] When surfactant is present, ΔG_s becomes

$$\Delta G_s = (\epsilon + \gamma)\frac{2B^2\pi^2}{\Lambda} - \Lambda B^2 \frac{d\Pi}{dh} \tag{3a}$$

$$\epsilon = \frac{d\gamma}{d(\ln a)} = \epsilon_d + i\eta_s\omega \tag{3b}$$

where ϵ is the surface dilatational modulus, ϵ_d and η_s are the elastic and shear dilational moduli, ω is the frequency of the disturbance (note: $\epsilon_d \approx \epsilon_0$ when $\omega \rightarrow \infty$), B is the amplitude of the disturbance, and Λ is its wavelength. The second term in eq 3a accounts for the change in interaction energy accompanying the disturbance and is normally a small contribution to the overall energy change.[41] The difference between eq 3 and Vrij's classical expression is the surface modulus term which arises from having surfactant adsorbed to the interface. Higher order surface curvature terms can also be incorporated into the analysis, but they are typically small in comparison to ϵ and γ.[46] Since the surface modulus (i.e. elasticity) may in some cases exceed the initial surface tension, it can actually become the most influential contribution to the disturbance. Hence, with reference to eq 2 we see that high surface moduli decrease the probability of the disturbance (i.e. *dampen spatial fluctuations*). The hydrodynamic influence associated with this surface moduli effect is often qualitatively expressed as a Gibbs−Maringoni stabilization mechanism. Long ago Lucassen and Hansen demonstrated experimentally that surfactant monolayers do indeed have a strong dampening effect on surface fluctuations.[47]

The film size can also have an influence on the energetics of the spatial fluctuations. This effect was originally identified by Vrij and is revealed in eq 3 by scaling the film diameter with the wavelength of the disturbances. In summary, for very small films Λ will be restricted by the film diameter, and consequently only short wavelength disturbances are possible. Thus, when the film dimensions restrict the wavelength for a disturbance, a fixed amplitude wave will expend more energy and the disturbance will be less probable in these wavelength-restricted films. That is, small metastable CBF films should be less susceptible to spatial fluctuations and hence show an increased stability. The actual film size where this becomes important depends on the system; however, Vrij has shown that spatial fluctuations can be significantly dampened in micron-sized films.[39,40]

Surfactant Density Fluctuations. Surfactant density fluctuations at the interface, Figure 8b, are also not accounted for in a classical DLVO approach. For ionic surfactants these fluctuations induce charge fluctuations which can influence the local height of the DLVO barrier, $\Delta\Pi_{max}$. A similar study showing how a fluctuating barrier height increases particle coagulation kinetics indicates that these fluctuations may also be important in the rupture process of foam and emulsion films.[48−50] Applying

(42) Derjaguin, B. V.; Prokhorov, A. V. *J. Colloid Interface Sci.* **1981**, *81*, 108.
(43) Kashchiev, D.; Exerowa, D. J. *Colliod Interface Sci.* **1980**, *77*, 501.
(44) Kabalnov, A.; Wennerström, H. *Langmuir* **1996**, *12*, 276.
(45) Rusanov, A. I. *Colloid J. USSR* **1966**, *28*, 445, 583.
(46) Schmelzer, J. W. P.; Gutzow, I.; Schmelzer, J. *J. Colloid Interface Sci.* **1996**, *178*, 657.
(47) Lucassen-Reynders, E. H.; Hansen, In *Anionic Surfactants*; Lucassen-Reynders, E., Ed.; 1981; Surfactant Science Series, Vol. 11, p 173.
(48) Prieve, D. C.; Lin., M. M. J. *J. Colloid Interface Sci.* **1982**, *86*, 17.
(49) Adamczyk, Z.; Czarnecki, J.; Warszynski, P. *J. Colloid Interface Sci.* **1985**, *106*, 299.
(50) Warszynski, P.; Czarnecki, J. *J. Colloid Interface Sci.* **1989**, *128*, 137.

a standard statistical thermodynamic approach to the interface provides a simple method for investigating which properties influence surfactant density fluctuations at the air−water interface.[51] Analogous to bulk density fluctuations surface density fluctuations can be expressed by the following[52]

$$\frac{\langle(\Delta\Gamma)^2\rangle}{\langle\Gamma\rangle^2} = \frac{kT}{\Gamma^2 a}\left(\frac{\partial\Gamma}{\partial\mu}\right)_T \tag{4}$$

where the right-hand side of eq 4 represents the mean square relative deviation from the mean of the surfactant adsorption, μ is the chemical potential, and a is the area over which the surface fluctuation is considered. In addition, surface thermodynamics provides the following relation:

$$\left(\frac{\Gamma}{\partial\mu}\right)_{T,N} = \frac{\Gamma^2}{\epsilon_0}$$

Substitution of this expression into eq 4 reveals a direct analogy between the role played by the surface elasticity (i.e. Gibbs elasticity) and the bulk compressibility in modulating density fluctuations.

$$\text{adsorption density fluctuations} \quad \frac{\langle(\Delta\Gamma)^2\rangle}{\langle\Gamma\rangle^2} = \frac{kT}{\epsilon_0 a} \tag{5a}$$

$$\text{bulk density fluctuations} \quad \frac{\langle(\Delta\rho)^2\rangle}{\langle\rho\rangle^2} = \frac{kT\kappa}{v} \tag{5b}$$

Here ρ represents the bulk density, κ is the bulk compressibility factor, and v the volume. This analogy demonstrates the notion that compressibility is inversely related to elasticity.

Finally, we can express the probability of having a given fluctuation, P_Γ, by[52]

$$P_\Gamma \approx c_\Gamma \exp\left(-\frac{\Delta\Gamma^2}{2\langle\Delta\Gamma^2\rangle}\right)$$

and with the help of eq 5a we find that the probability to expose a bare surface of the size a, as depicted in Figure 8b, becomes

$$P_\Gamma \approx c_\Gamma \exp\left(-\frac{\epsilon_0 a}{kT}\right) \tag{6}$$

de Gennes has shown that eq 6 can also be obtained by applying a classical thermodynamic approach.[53] The charge fluctuations associated with the surfactant density fluctuations described by eq 6 will likely become important when a is on the order of the film thickness and when the time scale for film rupture (or transition) is close to that of the fluctuation period. Important to note from eq 6 is that high surface elasticities will diminish the probability of surfactant density fluctuations and thus produce films less sensitive to this phenomena.

Although eqs 2 and 6 are somewhat qualitative and only consider thermally induced fluctuations, they do provide important physical insight concerning film rupture. Both equations indicate that the surface elasticity plays a key role in dampening both spatial and density fluctuations in foam and emulsion films. When these fluctuations are dampened the probability of overcoming the activation barrier which holds a film in a metastable state is lower and the film will be more stable. Equations 2 and 6 solidify the intuitive notion that not only is the height of the activation barrier important, but also the system's ability to resist disturbances. In addition, these simplified expressions provide a clear picture of how the surface elasticity influences the energetics of the film-rupture process. Whether or not disturbances are thermally or mechanically induced, a cohesive surfactant monolayer with a high surface elasticity will promote film stability.

Table 2. Hydrocarbon-Chain Parameters for C_nTAB Air−Water Monolayers

	l_c (Å)	σ_c (±1 Å)[a]	σ_{corr}[a]
C_{10}TAB	14.2	17.0	
C_{12}TAB	16.7	16.0	11.5
C_{14}TAB	19.0	16.0	11.0
C_{16}TAB	21.7	16.5	10.0

[a] Values obtained from Thomas et al.[21−28]

Stability of C_nTAB Foam Films. As shown earlier the DLVO force profiles for our C_nTAB films cannot fully account for the observed film stabilities. In light of the discussion pertaining to surface fluctuations and film rupture, it is also pertinent to evaluate the C_nTAB monolayer properties for these films. Fortunately, two excellent studies concerning C_nTAB monolayers at the air−water interface already exist. In an unprecedented series of papers, Thomas et al. have extensively characterized the equilibrium structure of C_nTAB monolayers using neutron reflectivity,[21−28] while Joos et al. provide relevant dynamic surface adsorption properties.[19,20] Taken together with the present results, a clear picture of how the surfactant chain length and monolayer structure influence film stability starts to emerge.

In Table 2 we reproduce some of the structural parameters for the C_nTAB (cmc) air−water monolayers deduced by Thomas et al.[21−28] Again, σ_c represents the width of the Gaussian chain distribution (see Figure 1) and l_c corresponds to the fully extended surfactant chain length.[54] Chain distribution widths corrected for surface roughness, σ_{corr}, are also provided in the table (see ref 28 for details). As shown in Table 2, Thomas et al. find that the most striking feature revealed upon comparing C_nTAB monolayers is that after increasing the chain length beyond C_{10}TAB, "*the width of the chain region, σ_c, hardly changes with the length of the chain.*" In addition, C_{10}TAB, which has the shortest chain, gives the thickest hydrocarbon layer. Thus C_{10}TAB is thought to have the most loosely packed monolayer with highly staggered chains. For C_{12}TAB, $l_c \approx \sigma_c$ and the chains are slightly packed but near full extension. After C_{12}TAB the hydrocarbon layer thickness remains constant and its density (i.e. packing) increases with surfactant chain length. From these results it is concluded that "*the cohesion energy of the chains is an important factor in determing the structure of the layer.*" This conclusion is remarkably coincident with our film stability observations in relation to surface fluctuations. Although the C_{10}TAB and C_{12}TAB monolayers produce highly charged interfaces, which in turn generate relatively high activation barriers to rupture, the surface layers are not cohesive enough to protect the film from fluctuations and consequently the films are unstable. Further increases in surfactant chain length to C_{14} and C_{16} produces much denser hydrocarbon layers at the interface (with a head group area nearly equivalent to the lower chain lengths) and very stable films. The

(51) Erickson, J. C. Private communication.
(52) Hill, T. L. In *Statistical Mechanics Principles and Selected Applications*; McGraw-Hill: New York, 1959; Chapter 4, p 97.
(53) de Gennes, P. G. Private communication.
(54) Tanford, C. J. *J. Phys. Chem.* **1974**, *78*, 2649.

Table 3. Interfacial Parameters for C_nTAB Air−Water Monolayers

	ϵ_0	ϵ_{200}	ϵ_{700}	k (s^{-1})	k_1	k_2
C_{10}TAB	45			1100	0.47	2.0
C_{12}TAB	47	6.1	9.8	900	1.5	1.7
C_{14}TAB	61	16.3	39.5	480	3.4	1.4
C_{16}TAB	61					
C_{14}TAB +11 mM KBr				430	2.8	1.0

[a] ϵ_0 = Gibbs elasticity values in mN/m, k_1 = adsorption rate constant in 10^{-2} cm/s, and k_2 = desorption rate constant in 10^{-8} mol/cm·s. In every case the surfactant concentration is equal to the salt-free cmc and all k, k_1, and k_2 values are taken from ref 19.

higher film stability displayed by these longer chain surfactants likely arises from their stronger cohesive properties and ability to resist fluctuations. The C_{12}TAB films can also be made stable by adding small amounts of a long chain alcohol, which increases the cohesion (i.e. elasticity) within the monolayer. Interestingly, since the uncharged alcohol molecules displace the surfactant at the interface,[55] thereby lowering the surface charge, classical DLVO principles would predict a decreased stability upon the addition of alcohol. Here again the augmented film stability appears to be a consequence of increasing the cohesion of the monolayer.

The dynamic monolayer properties for these cationic surfactants also indicate an increase in monolayer cohesion with surfactant chain length. C_nTAB surface elasticity results, together with some of the air−water surfactant-exchange-rate data obtained by Joos et al. are tabulated in Table 3. The surfactant exchange rates are deduced from dynamic surface tension measurements using the oscillating jet method, where k is the overall rate constant based on the kinetic model of Joos et al., k_1 is the adsorption rate constant, and k_2 is the desorption rate constant. ϵ_0 was obtained from our equilibrium surface tension isotherms while ϵ_{200} and ϵ_{700} are dilatational elasticity values, at 200 and 700 Hz, respectively, measured using the excited capillary waves techinque.[56,57]

Two important points can be noted from the rate constant data in Table 3. First, the exchange rate of C_nTAB monomers at the air−water interface is on the order of a millisecond, and second, the desorption rate is nearly constant while the adsorption rate dramatically increases with increasing surfactant chain length. Joos et al. attribute the later to the hydrophobic effect.[19] Millisecond time constants are important because this is the same characteristic time found from a nonlinear hydrodynamic analysis for film rupture.[58] Overlap of these time scales suggests that density fluctuations can play a role in the rupture process. In addition, the higher adsorption rates of the longer chain surfactants indicates a stronger tendency for these surfactants to adhere to the interface (i.e. the longer chain length surfactants are more surface active).

Along with the higher surface activity of the longer chain length surfactants, there is also an increase in surface elasticity with carbon chain length (see Table 3). This is true for both the Gibbs elasticity and the lower frequency elasticities measured with excited capillary waves. We find that C_{10}TAB and C_{12}TAB have practically identical Gibbs elasticities at the cmc (46 mN/m), while there is a 30% increase observed upon extending the chain length to C_{14}TAB and C_{16}TAB (61 mN/m). Figure 5 also reveals that at surfactant concentrations equal to the same percentage of the cmc, the longer chain length surfactants consistently display much higher Gibbs elasticities. Furthermore, excited capillary wave measurements at the cmc show that there is an even more dramatic increase in the dilatational elasticity between C_{12}TAB and C_{14}TAB at 200 and 700 Hz. During these capillary wave measurements it was also noted that extremely high elasticities were produced by trace amounts of surface active contaminants.[57] In accord with the trends predicted by eqs 4 and 6, all of the elasticity data support the film stability differences seen with increases in the surfactant chain length.

Conclusion

A systematic study of the forces and stability of foam films generated from a homologous cationic surfactant series, alkyltrimethylammonium bromide surfactants (C_nTAB, n = 10, 12, 14, 16), has been carried out. By using this surfactant series we are able to obtain quantitative surface force measurements between tertiary alkylammonium bromide monolayers while simultaneously investigating the effect surfactant chain length has on the forces and stability of thin-liquid films. These objectives are accomplished by measuring the surface tension and disjoining pressure isotherms for each surfactant. In addition, we utilize previously published neutron reflectivity[21−28] and dynamic surface tension data[19,20] to relate our measurements and observations to the structure and properties of the surfactant monolayers at the air−water interface.

Applying a standard DLVO analysis to the disjoining pressure data permits us to compare our force curves to those published for alkylammonium bromide bilayers. The effective surface charge densities and ionization constants found are in good agreement with previously reported values. In all cases the charge densities are rather low, ~0.05 C/m^2, and we deduce a correspondingly low ionization of the surfactant monolayers, ~10%. Significant in this work is that the surfactant adsorption at the air−water interface is accurately known from both surface tension and independent neutron reflectivity measurements of Thomas et al.; therefore, no assumptions concerning the surfactant molecular area are used to determine the degree of ionization. Furthermore, the excellent agreement between the surface tension and neutron reflectivity adsorption results (Figure 4) represents an extensive verification of the Gibbs adsorption equation. The surfactant density profiles determined by Thomas et al. also suggest that the low ionization constants observed may in part be due to the diffuse structure of the surfactant monolayers.

We also find that the surfactant chain length can have a significant effect on foam film stability. For highly purified surfactant solutions there is a sharp increase in film stability when increasing the chain length from C_{12} to C_{14}. Purified C_{12}TAB films display low rupture pressures (<1 kPa) in comparison with C_{14}TAB and C_{16}TAB (>30 kPa). Furthermore, C_{10}TAB films where so unstable we could not even obtain meaningful metastable pressure versus thickness measurements. Interestingly, C_{12}TAB film stability can be made equivalent to that of the C_{14} and C_{16} chain length surfactants if small amounts of a long-chain alcohol (C_{12}OH) are added or if the surfactant is left unpurified. All similar efforts to stabilize the C_{10}TAB surfactant films failed, and these films always remained very unstable. Neutron reflectivity, dynamic surface tension, and surface elasticity measurements all indicate that the differences in film stability originate from the cohesive properties of the surfactant monolayer;

(55) Penfold, J. *Prog. Colloid Sci.* **1990**, *80*, 198.
(56) Stenvot, C.; Langevin, D. *Langmuir* **1988**, *4*, 1179.
(57) Giermanska-Kahn, J. Private communication.
(58) Williams, M. B.; Davis, S. H. *J. Colloid Interface Sci.* **1982**, *90*, 220.
(59) Hwang, C. C.; Chang, S. H.; Chen, J. L. *J. Colloid Interface Sci.* **1993**, *159*, 184.

strong cohesion promotes film stability by dampening spatial and density fluctuations at the interface. A higher cohesion in the longer chain surfactant monolayers is evidenced by a faster monomer adsorption rate constant, higher Gibbs and dilatational surface elasticities, and denser hydrocarbon layers. The later point is revealed by the width of the chain distribution, σ_c, measured from neutron reflectivity (see Table 2). After the chain length increased beyond C_{10}, the width of the chain region hardly changes. Thus C_{10}TAB, which has the shortest chain, gives the thickest layer and produces a very loosely packed monolayer. For C_{12}TAB the chains are slightly packed but near full extension. After C_{12}TAB the hydrocarbon layer thickness remains constant, and its density (i.e. packing) increases with surfactant chain length.[28]

Consistent with Thomas et al.'s neutron reflectivity results, a more cohesive monolayer for the longer chain length surfactants is revealed by their increased surface elasticities. The Gibbs elasticity for C_{10}TAB and C_{12}TAB is nearly equal, but there is a 30% increase seen for C_{14}TAB and C_{16}TAB. An even more profound difference between C_{12}TAB and C_{14}TAB is observed for surface dilatational elasticities at 200 and 700 Hz. Finally, we note that C_{12}TAB films made stable by adding small amounts of a long-chain alcohol provide further evidence that an increase in the elasticity (i.e. cohesion) of the monolayer promotes film stability. Clearly repulsive forces are needed to produce the activation barriers trapping a thin film in a metastable equilibrium, and high barriers favor film stability; however, monolayer cohesion plays a crucial role.

Although a complete theory for nucleated rupture of CBF films has yet to be developed, it is likely that fluctuations play an important role. Equations 4 and 6 demonstrate that both spatial and surfactant density fluctuations at the interface strongly depend on the surface elasticity; high elasticities dampen both types of fluctuations. Foam film stability observations obtained for the C_nTAB solutions tested here provide fundamental evidence that increasing the chain length for soluble surfactants or adding a cosurfactant can stabilize films by producing denser, more cohesive monolayers at the air−water interface.

Acknowledgment. The author thanks B. Cabane, P. G. de Gennes, and J. C. Erickson for many fruitful discussions. In addition J. Giermanska-Khan is thanked for providing her excited capillary wave data and Rhône Poulenc for partial financial support.

LA970004Q